NEW Fe I LEVEL ENERGIES AND LINE IDENTIFICATIONS FROM STELLAR SPECTRA. III. INITIAL RESULTS FROM UV, OPTICAL, AND INFRARED SPECTRA

Ruth C. Peterson
SETI Institute, 339 Bernardo Ave., Suite 200, Mountain View, CA 94043
e-mail: peterson@ucolick.org

Robert L. Kurucz
Center for Astrophysics | Harvard & Smithsonian, 60 Garden Street, Cambridge, MA 02138

Short title: New Fe I Energies and Line Identifications Incorporating Stellar Infrared Spectra

ABSTRACT

The spectrum of neutral iron is critical to astrophysics, yet furnace laboratory experiments cannot reach many high-lying Fe I levels. Instead, Peterson & Kurucz (2015) and Peterson, Kurucz & Ayres (2017) turned to UV and optical spectra of warm stars to identify and assign energies for 124 Fe I levels with 1900 detectable Fe I lines, and to derive astrophysical gf-values for over a thousand of these. An energy value was assumed for each unknown Fe I level, and confirmed if it shifted the predicted positions in updated Kurucz (2011) Fe I calculations to match exactly in wavelength the positions of four or more unidentified lines in the observed spectra. Nearly all these identifications were for LS levels characterized by spin-orbit coupling, whose lines fall primarily at UV and optical wavelengths. This extension of these searches provides a hundred new Fe I level identifications. Forty LS levels are identified largely by incorporating the positions of unidentified laboratory Fe I lines with wavelengths < 2000 Å. Adding infrared spectra provided sixty Fe I jK levels, where a single isolated outer electron orbits a compact core. Their weak, blended lines fall mostly in the infrared, but are searchable because their mutual energies obey tight relationships. For each new Fe I level, this work again provides and makes publicly available its identification, its energy, and a list of its lines with theoretical gf values. For suitably distinct lines, this work also includes astrophysical gf-values, ones adjusted semi-empirically to fit the stellar spectra.

1. OVERVIEW

This work continues investigations by Peterson & Kurucz (2015; hereafter PK15) and Peterson, Kurucz, & Ayres (2017; hereafter PKA17) to derive new identifications and energies for Fe I levels that are too highly excited to have been determined in earlier laboratory and solar analyses. These two works adopted a wide range of stellar spectra observed in the UV and optical wavelengths as the "laboratory" source to seek levels whose lines were strong and isolated enough to be distinctly discerned. Matching four lines predicted for each level to observed wavelengths with a single energy shift determined the new level energy and its identification. In this work, incorporating laboratory positions for unidentified lines with wavelengths < 2000 Å and adding infrared spectra of the Sun and the cool giant Arcturus has enabled the determination of a hundred new Fe I levels. Their energies, identifications, and associated Fe I lines, including astrophysical gf-values where feasible, are presented here and made publicly available.

Section 2 summarizes the importance of extending Fe I level identifications, and the procedure and the results of previous work. Section 3 describes the identification of forty new levels, found primarily by adding the laboratory positions of unidentified lines at wavelengths blueward of the useful range of stellar UV spectra. Section 4 outlines how incorporating infrared spectra can yield identifications for Fe

I levels of a different structure whose lines fall primarily in the infrared. Section 5 presents the infrared spectra adopted, and Section 6 discusses the calculation of infrared spectra to match them. Section 7 describes modifications to the search procedure adopted in the infrared. Section 8 summarizes the results, and Section 9 describes the status, prospects, and impact of the identification of Fe I levels.

2. PREVIOUS WORK

Astrophysical observations are dramatically improving. New cosmic surveys are recording a plethora of ever-fainter sources. Automated analysis offers the promise of rapid interpretation. Often lacking, however, are the laboratory astrophysics data needed to analyze the new observations. These are the basic atomic and molecular parameters necessary to model at all wavelengths, from ultraviolet (UV) to infrared (IR), the spectral absorption and emission of supernovae, nebulae, and the hot outer layers of stars and their galaxies, at both low and high redshifts.

Especially critical are line parameters for the neutral iron atom, due to its high cosmic abundance and its complex line spectrum. In the Sun, the Fe I lines of neutral iron have long been known to dominate both the optical region (e.g. Moore et al. 1966) and the UV (e.g. Tousey 1988). While energy levels, wavelengths, and transition probabilities (gf-values) can often be derived theoretically for light, simple atoms, the Fe I spectrum is best characterized observationally. From a laboratory furnace, Brown et al. (1988; hereafter B+88) provided determinations of wavelengths of Fe I spectral absorption in the UV and optical regions. Nave & Johansson (1993a,b) then provided Fe I level energies up to ~60800 cm^{-1} with uncertainties <0.005 cm^{-1}, and wavelengths for over 2000 Fe I lines from 1700Å to 5 μm. They noted that a myriad of lines of high-lying unidentified Fe I levels still remained in the solar spectrum.

In the ~2000K laboratory furnace, the population of highly-excited Fe I levels is severely depleted by the exponential Boltzmann temperature dependence. In contrast, stars at ~6000K like the Sun are warm enough to significantly populate these levels without overly ionizing Fe I to Fe II. In the spectra of such warm stars, the resulting multitude of unidentified Fe I lines leads to poor spectral modeling, notably a serious underestimate of observed UV flux distributions by calculations that lack them (PK15, Fig. 1).

Fe I level energies can be predicted through quantum-mechanical calculations. For example, Kurucz (2011, 2017, 2018) has run least-square fits based on the Cowan (1981) codes to predict whole Fe I transition arrays and the resulting wavelengths and gf-values of the lines of each level across all wavelengths. However, these are not nearly as accurate as laboratory derivations, due to the complexity of the Fe I atom and mixing in the eigenvectors that characterize each level. Owing to the sizable errors in theoretical level energies, adopting these theoretical wavelengths leads to typical errors of 10Å in the UV and 100Å in the IR.

The predicted line parameters suffice for modeling low-resolution flux distributions of stars across a wide temperature range, but are woefully inadequate where discernment of lines of other species is essential. This is critical for many research areas, such as two recently reviewed by Matteucci (2021): the assembly of the Galaxy following galactic nucleosynthesis and star formation at the earliest epochs (e.g. Sneden, Cowan, & Gallino 2008), and the corresponding origin and development of the Galactic bulge (Ryde et al. 2016; Barbuy et al. 2018). Unrecognized absorption by unidentified Fe I lines may lead to abundance overestimates for abundances of critical trace elements whose lines occur only in the UV (Peterson, Barbuy, & Spite 2020; Peterson 2021). As discussed in Sec. 9, their presence affects the placement of the infrared continuum in strong-lined giants such as those of the Galactic bulge (e.g. Ryde et al. 2016, Fig. 3). Identifying unknown Fe I lines is thus critical to facilitate the total scientific harvest from existing high-resolution spectrographs, even those with resolution ~50,000 such as Keck

HIRES (Vogt et al. 1994) and CRIRES (Käufli et al. 2004), and from those under development such as the ELT-HIRES spectrograph (Maiolino et al. 2013).

Consequently, PK15 and PKA17 adopted UV and optical spectra of warm stars as the "laboratory source". Extending the approach of Castelli & Kurucz (2010) to identify Fe II levels in a single hot B star, these authors compared the observed optical and UV spectra of a variety of warm and cool stars with theoretical synthetic spectral calculations generated with the Kurucz (1993) program SYNTHE that were run for each individual star. The atmospheric models for these calculations were interpolated in the model grid of Castelli & Kurucz (2003) to the parameters given in Table 1 of PK15. The line parameters input to these calculations were constructed from the Kurucz (2011) list for known (but not predicted) Fe I lines, along with Kurucz line lists for other species, both atomic and molecular. To better reproduce the observed line strengths, atomic gf-values in the original lists were revised line-by-line, while those for molecules were altered by band.

To identify a particular unknown level, its identification was adopted from the Kurucz (2011) Fe I quantum-mechanical calculations based on the precepts of Cowan (1981). An energy was simply assumed; it was confirmed if the resulting adjusted positions of at least four of its associated predicted spectral lines matched the exact wavelengths of at least four unidentified lines in all relevant stellar spectra. Furthermore, a single adopted gf-value for each such line, which was usually modestly lower than the predicted value, had to provide a calculated strength that matched approximately the observed strength of that line in each stellar spectrum. As Sec. 1 of PKA17 emphasizes, the observed spectra deliberately spanned a wide range in both line strength and stellar temperature; matching all their strengths simultaneously provided a more stringent test than matching a few similar spectra. Once four such line matches had confirmed the new identifications of about twenty Fe I levels, the Kurucz Fe I predicted calculations were run again. This significantly improved the predicted energies, wavelengths, and gf-values for the next round of Fe I searches. Following this procedure, these two publications provided identifications and energies for a total of 124 previously unidentified Fe I levels, resulting in nearly 3000 detectable lines in the UV/optical and a similar number of lines likely detectable in the IR.

3. LEVELS WHOSE LINES FALL PRIMARILY IN THE UV AND OPTICAL

Nearly all the previous Fe I identifications were for LS levels, whose structure is characterized by spin-orbit coupling. Lines of LS levels are strongest in the UV and optical, so the preceding works targeted levels with strong lines in relatively unblended sections of these regions. The remaining unidentified levels tend to have weaker lines, or strong lines that fall in heavily obscured UV regions. Two of the latter regions are at wavelengths below 2000 Å and the 2600 – 2700 Å region shown in Fig. 1 of PK15. Peterson et al. (2020, Sec. 5) demonstrated that the former region is heavily blanketed by unidentified Fe I lines of high-excitation levels of odd parity, whose lower even-parity levels lie near the ground state, and that their even-parity counterparts populate the latter region, since the lowest odd-parity Fe I levels fall well above the ground state.

At wavelengths < 1900 Å, the declining quality and increased blending of even the spectra of weak-lined stars limits the success of searches for further Fe I level identifications (PKA17, Sec. 6). Figs. 1—3 of Peterson et al. (2020) illustrate directly how the crowding of unidentified lines coupled with the low signal-to-noise in the stellar spectra make line identification difficult. However, due to the low excitation levels of Fe I lines in this region, the laboratory furnace provides a valuable resource. The present work has taken advantage of the laboratory Fe I line positions in this region, especially those for which B+88 could not make a definitive identification, but could provide a lower and upper energy and J value, based on the spacing in wavelength at successively increasing lower levels of excitation.

Incorporating these B+88 lines and levels provided identifications for nearly three dozen Fe I levels that otherwise had too few UV and optical stellar spectral line matches. To identify fully a B+88 level assigned an energy E and angular momentum J, a predicted level was selected of the same J and similar E whose UV line gf-values, when reduced to reflect the population of the lower level at the 2000K furnace temperature, provided consistency with the B+88 line intensity measurements. The level energy was assigned accordingly; agreement to 0.02 cm^{-1} to the B+88 line positions was demanded in the shifted predicted line positions. Each such match was counted as a line detection. Levels with only three detections were accepted when no other LS level with the same J and a predicted energy within ±150 cm^{-1} remained unassigned. In addition, several levels with at least one line detected at longer wavelengths were identified by similarly matching B+88 lines for which no J nor energy was provided.

Thirty-four of the forty new LS level identifications were made in this way, all for levels of odd parity. The largest difference between the predicted and adopted energy of a new LS level was 269.8 cm^{-1}. For all the others this difference was below 200 cm^{-1}, and exceeded 150 cm^{-1} for only three of these.

The remaining six new LS identifications relied as before on stellar lines present across the entire spectrum. Three met the PK15 and PKA17 criteria directly. Three others with J>6 were accepted but with only two matches, since each match was made for an unusually strong line with a high gf-value. All but one of these six newly identified LS levels are also of odd parity.

Among levels of even parity, similar checks of LS levels with large differences between observed and predicted energies led to the rejection of one level and the reassignment of the energy of two levels identified by PKA17. Among levels of odd parity, applying the procedures for jK levels described below in Sec. 7 necessitated changes for published jK levels as well. Table 1 lists these revisions.

4. LEVELS WITH LINES IN INFRARED STELLAR SPECTRA

In solar-type stars, almost all unidentified UV/optical Fe I lines arise from a transition to an unknown upper level from a known low-lying level. The line strength depends on the population of the low level, which is only modestly diminished at these temperatures by the exponential energy dependence of the Boltzmann factor. However, unidentified Fe I lines also appear in the infrared (IR), beyond 1μm. These arise from two high levels, one or both of which may be unknown. In either case, these unidentified Fe I IR lines are rather weak. The absorbing population is diminished by the Boltzmann factor of the lower level, which is usually at high energy since the vast majority of Fe I levels at lower energy are known. Consequently, unidentified lines in infrared spectra of stars of solar temperature and cooler are much weaker than the unidentified UV and optical lines studied previously. Infrared searches thus demand higher accuracy, in both the observational spectra and in the theoretical spectral calculations.

Including infrared spectra nonetheless assists such searches, as discussed and illustrated in Section 5 and Figure 1 of PKA17. Infrared spectra not only expand the number of potential line detections for a given level, but also provide a more accurate determination of the level energy. The latter arises because the spectral line profile in the relevant wavenumber (energy) space narrows steadily to the red: the stellar line profile is constant in velocity space, and so varies as $\delta\lambda/\lambda$.

Furthermore, infrared spectra enable the determination of Fe I levels with a different atomic structure. The newly-identified levels described in Sec. 3, and virtually all the levels identified by PK15 and PKA17, have LS coupling, the spin-orbit interaction between the outer and innermost electrons of neutral iron. Incorporating infrared stellar spectra in this work, especially those of the Sun, has opened up the determination of energies for levels represented by jK coupling, in which a core configuration is accompanied by a single, relatively isolated electron. Such levels rarely have distinct UV lines, but

have a myriad of infrared lines, the vast majority of which are weak.

5. SELECTION OF INFRARED STELLAR SPECTRA

The very high-quality IR spectra of the Sun provided the greatest number of jK line detections. Infrared spectra of two cool giants, especially that of the mildly metal-poor giant Arcturus, were also consulted to distinguish whether a particular unidentified feature is indeed due to Fe I, and to sort out contamination by other low-excitation lines.

The limited number of infrared stellar spectra searched arose from three aspects pertinent to infrared but not UV-optical Fe I searches. *a*) In the infrared, unidentified Fe I lines become very weak, for the population of the lower level is reduced by its substantially higher excitation (Sec. 4). Consequently, high signal-to-noise and spectral resolution are especially crucial. By these criteria, the Sun is by far the best-observed star in the infrared. *b*) Infrared spectra obtained from the ground are strongly affected by absorption by the Earth's atmosphere, which appears sporadically across a wide range of infrared wavelengths and blocks some broad regions completely (Hinkle et al. 1995, Table 3). Space-based spectra of the Sun were adopted where available; elsewhere, ground-based spectra for the Sun and Arcturus were adopted that attempted to correct for this absorption. *c*) Strong molecular absorption occurs throughout the infrared in spectra of cool giants such as Arcturus (Hinkle et al. 1995, Table 5), and is much weaker but nonetheless present in the solar infrared spectrum as well. The Arcturus spectrum provides a useful comparison to judge whether a given absorption feature in the solar spectrum is blended (or obliterated) by molecular absorption. The spectrum PKA17 adopted for the red horizontal branch star HD 95870 was also included where it was available. However, spectra of the cooler, metal-rich giant μ Leo (HD 85503) were not used because of strong molecular contamination, notably that of CN.

A comparison of the spectra of the Sun and Arcturus was very useful to reveal the atomic species giving rise to a particular absorption feature or blend. Mildly metal-poor, Arcturus has high abundances with respect to iron of several atomic species such as Mg I, Si I, and Ca I (e.g. Peterson, Dalle Ore, & Kurucz 1993), whose lines are significantly present in the infrared (Hinkle et al. 1995, Table 4). Fig 1*b* of PKA17 illustrates that, while the Fe I line at 1776.5234 nm is about the same strength in the spectra of the Sun and Arcturus, the Mg I lines near 1774.96, 1775.4, and 1776.2 nm all become much stronger in Arcturus than in the Sun. In contrast, HD 95870 has near-solar abundances (Afşar et al. 2018).

For the Sun, for wavelengths beyond 2.1μm, telluric-free FTS spectra are available from two space missions designed to secure high-resolution spectra of the earth's atmosphere: ATMOS (Farmer & Norton 1989; Abrams et al. 1996) and ACE (Hase et al. 2010). Their spectral coverage is similar (ATMOS: 625 – 4800 cm^{-1}; ACE: 750 – 4400 cm^{-1}). The ACE spectrum generally achieved a higher signal-to-noise ratio S/N, but at a lower resolution, 0.02 cm^{-1} for ACE versus 0.01 cm^{-1} for ATMOS. Both observations recorded the center of the solar disk with an aperture 10 – 15% of the solar diameter. Many unidentified lines appear in both: Hase et al. report in reference [2] that 2400 newly identified lines in the ACE spectrum were published in 1995, and an additional unpublished 2700 lines in 1998.

The ACE spectrum was downloaded from its mission website, and included the plot of the atlas, in which many lines identified by L. Wallace are labeled; the two files of identified and unidentified lines; and the ASCII digital data file. The ACE digital data file provides pairs of wavenumber versus normalized intensity suitable for direct comparison against calculated spectra. Reduction of the individual FTS ATMOS strips into such pairs was accomplished by Kurucz. The ATMOS spectra have higher S/N than the ACE spectra at their bluest wavelengths, but its S/N declines below that of ACE

redward of ~2.5 μm. Wherever both spectra existed, both were frequently consulted to confirm line detections; the higher resolution of the ATMOS spectra was often critical in disentangling line blends.

At shorter wavelengths, ground-based solar intensity spectra of the center of the solar disk were downloaded from the National Solar Observatory (NSO) website of Kitt Peak National Observatory (KPNO). The atlas of Wallace, Hinkle, & Livingston (1993) was adopted over 730 – 11230 Å, and that of Wallace & Livingston (2003) from 11230 – 20830 Å. For each atlas, telluric spectrum removal was accomplished for all but the strongest line regions, based on a sequence of solar spectra obtained over a wide range of air mass.

Wallace et al. (2011) have provided a similarly high-resolution, high-S/N solar flux spectrum that includes light from the entire disk of the Sun, from which the telluric spectrum is also removed. They note that the solar flux spectrum is better suited as a standard for comparison against stellar spectra, which are necessarily flux spectra since stars are not spatially resolved. However, Figure 1 of Wallace et al. (2011) reveals that Fe I line profiles at disk center are sharper and deeper than those of the flux spectrum, and thus better suited to the present purpose. Unlike the flux spectrum, that of the disk center is free from the degradation in resolution engendered by the solar rotational velocity of 2 km s^{-1}. Moreover, the disk-center spectrum is obtained at an angle perpendicular to the solar photosphere, which provides deeper penetration into the hotter solar layers that favor high-excitation Fe I line formation.

For Arcturus, two ground-based spectra were adopted: the Hinkle et al. (2000) atlas over 730 – 9120 Å, and the Hinkle et al. (1995) atlas from 9100 Å to 5.3 μm. These were obtained with the FTS on the KPNO 4m telescope. Telluric removal for the Hinkle et al. (2000) atlas relied on the procedure and spectra noted above for the Sun. In the infrared, Section 2.2 of Hinkle et al. (1995) describes how the Arcturus observations were scheduled to optimize telluric removal by maximizing the difference in the stellar geocentric velocity. The resulting Summer and Winter Arcturus spectra achieved a maximal displacement of 45 km s^{-1} (0.6 cm^{-1} at 4000 cm^{-1}), enough to readily distinguish individual absorption lines in Arcturus from those of the telluric spectrum.

The solar and Arcturus ground-based spectra were converted to wavenumber-intensity/flux pairs suitable for plotting using the NOAO data reduction package IRAF. The tilt of each segment was removed to allow the end of one segment to agree with the beginning of the next, and the individual points in the overlap region were averaged. Regions or points that had experienced significant telluric contamination and showed extreme variations were removed. The two Summer and Winter spectra of Hinkle et al. (1995) were generally displayed individually at infrared wavelengths. At wavelengths < 11100 Å, the Summer spectrum alone was adopted, and was overplotted on the Hinkle et al. (2000) atlas for wavelengths where both were available.

6. INFRARED SPECTRAL SYNTHESIS

6.1 Calculations of Stellar Spectra in the Infrared

The spectral calculations followed the previous procedure, outlined in Section 5 of PK15 and further characterized in Section 3 of PKA17. Briefly, a one-dimensional (1D) radiative model atmosphere calculated in local thermodynamical equilibrium (LTE) of suitable temperature T_{eff}, gravity log g, and microturbulent velocity v_t for each star was selected from the Castelli & Kurucz (2003) ODFNEW grid. The solar model was that of PK15, whose Table 1 lists its parameters. The models for the two cool

giants Arcturus and HD 95870 were those described in Sections 3 and 5 of PKA17. Each model spectrum was then generated by incorporating into the Kurucz SYNTHE program a list of wavelengths and transition probabilities for atomic and molecular transitions that give rise to absorption features observed in spectra of solar-temperature dwarfs and cooler giants. Calculations were performed in wavelength space, to conform to the adopted line lists, but were converted to wavenumber space in the search plots, in which an energy offset is a linear shift. The spectral calculations were run from 6000 Å to 6μm (16700 to 1680 cm^{-1}) for each star. Plots for the search were generated by overplotting the observed spectra described above on these calculations. Fig. 1 of PKA17 provides an early example. From plots such as these, matches were sought to unidentified lines.

The SYNTHE program starts the spectral computation by calculating the radiative transfer through each of 17 rays of varying disk angle, from center to limb. For normal stars, SYNTHE then combines each ray with an appropriate offset dictated by the input stellar rotational velocity. This procedure, with zero rotation, was followed for the Arcturus spectral calculation. For the solar intensity spectral calculation, just the central ray calculation was retained. The microturbulent velocity v_t = 1.0 km s^{-1} adopted for the solar flux spectrum was reduced to 0.5 km s^{-1} for the disk center spectrum.

Spectral synthesis for this work in the infrared was thus extended beyond the limit of 8900 Å of PK15, and the exploratory calculations near 18000 Å shown in Fig. 1 of PKA17. To ensure representation of very weak lines in the infrared calculation, the initial input atomic line list for elements with atomic number $Z \leq 30$ relied almost exclusively on the Kurucz (2018) quantum-mechanical calculations of lines of a given species for which both energy levels are known. In particular, this list for Fe I includes numerous, very weak lines arising from jK levels. In contrast, Fe I jK lines are largely absent from the searchable database accessible through the NIST website. This is the primary source of atomic line parameters for many other theoretical spectral calculations, notably the Smith et al. (2021) update DR16 to the line list covering 15000 – 17000 Å (6670 – 5900 cm^{-1}) developed for the Apache Point Observatory Galactic Evolution Experiment (APOGEE; Majewski et al. 2017). Searches of the NIST database by wavenumber for Fe I returned none of the dozens of jK lines in Tables 3 and 4 of Schoenfeld et al. (1995), although this reference is included in the NIST Fe I bibliography.

The atomic line lists were downloaded from the Kurucz (1993) website from the subdirectory atoms under the subdirectory for each species, designated gf##*nn*.pos: ## = *Z,* and *nn* is the species ionization level, being 00 or 01 (neutral or singly-ionized) for the cool stars considered here. Where available, lists were ingested that begin with 'hyper' as these include hyperfine splitting, which becomes increasingly important in the infrared. For two species, lists were adopted that substitute laboratory gf values where they are available and appear to be improvements. For Mg I, gf1200.all was downloaded; for Na I, gf1100.all was updated from a download of *gfall08oct17.dat* from the Kurucz linelists/gfnew subdirectory. Since *gfall08oct17.dat* again includes hyperfine splitting for many species, it was also adopted for elements beyond Z = 30. For Ce II, the Cunha et al. (2017) list of nine H-band lines was incorporated. For Ba II, the Peterson et al. (2020) list developed by M. Spite incorporating isotopic splitting was adopted. Extensive revision to the calculated atomic gf values followed, to match the individual line strengths in each of the infrared stellar spectra adopted. This work is still underway.

6.2 Validity of the Spectral Modeling in the Infrared

Figure 1 plots (in wavenumbers) the observed spectra of the Sun and Arcturus superimposed on an earlier version of the infrared calculations described in Sec. 5 of PKA17. These calculations for each star are shown as blue lines. The solar ACE spectrum in the 3.5μm region is plotted as a green line. The

Hinkle et al. (1995) Arcturus observations in Summer and Winter are plotted as purple and orange lines; these are displaced downwards in Y by 0.1 for clarity. Along the top of the plot, the positions of selected lines of molecular and neutral atomic species are indicated by × for Fe I and by color-coded signs for other species. The diamonds beneath them highlight Fe I lines that arise from jK levels.

The ACE solar spectrum shown in Fig. 1 is of extremely high signal-to-noise. This proved essential to provide the large number of detectable lines needed to establish energies for sixty previously unidentified Fe I jK levels. A half-dozen jK lines fall within the 3.515 – 3.49μm wavelength region plotted in Fig. 2; they all arise from the s5f jK group of levels. One such line, at 2849.48 cm^{-1}, is from a level identified by Nave et al. (1994; hereafter N+94). The other five s5f lines are new identifications.

Regardless of their origin and identification status, all the absorption features in the solar spectrum over the region shown are weak. The Y-axis scale indicates that only the top 10% of the total intensity scale of the normalized solar spectrum is displayed. The calculations adopted Kurucz line lists that were generated prior to refined gf-value adjustment, so the synthetic spectrum is too strong for many lines, such as those between 2844 – 2848 cm^{-1}. Unidentified lines appear most clearly in the solar spectrum; they are revealed as absorption features seen in the green (observed) spectrum that are deeper than in the blue (calculated) spectrum. All but one of the blue diamonds appear directly above such features, which were not included in these early calculations. Since the s5f line at 2849.48 cm^{-1} was previously identified by N+94, this feature is matched by the calculation, and also has an × above it.

The figure also indicates the significant extent to which line blending impacts the profiles of both known and unknown lines. It illustrates that this blending must be modeled accurately to reliably detect unidentified lines and determine their position and strength.

6.3 Line-Strength Variations in Infrared Spectra

The Arcturus infrared spectrum is generally too noisy to show the weakest lines of Fe I. Moreover, systematic differences are seen between its Summer and Winter spectra, for example at 2844.16 cm^{-1} and 2847.48 cm^{-1}, where downward spikes appear in one Arcturus spectrum but not the other and no absorption line is seen in the Sun. Nonetheless the Arcturus spectra are useful to assess line blending.

Fig. 1*b* of PKA17 illustrates that, while the Fe I line at 1776.5234 nm is about the same strength in the spectra of the Sun and Arcturus, the Mg I lines near 1774.96, 1775.4, and 1776.2 nm all become much stronger in Arcturus than in the Sun. This arises in part because Arcturus abundances of Mg and other light elements are enhanced with respect to iron (e.g. Peterson et al. 1993). Farther to the infrared, Figure 1 indicates that the newly identified Fe I lines at 2844.68 cm^{-1} and 2856.59 cm^{-1} are mildly stronger in Arcturus than in the Sun. However, the line near the s5f Fe I line at 2850.19 cm^{-1} is much stronger, in both the Summer and Winter spectra. This and the offset of the s5f line profile from the observed line suggest the latter is largely due to a different species, one whose lines grow in strength in Arcturus, such as an Mg I line whose gf-value is too low. Any jK line as badly obscured as this one is not counted as detected in the search.

Fig. 1 indicates that molecular lines are also stronger in Arcturus. CH lines are more than twice as strong in Arcturus than in the Sun, while the OH molecular lines are nearly twenty times stronger. In the solar spectrum these CH and OH lines are of the same strength as many unidentified lines, but the Arcturus spectrum ensures they will not be mistaken for them.

The calculations bear out the somewhat surprising result that the strength of many unidentified Fe I lines are at least as strong in the Arcturus infrared spectrum as in the Sun (Fig. 1; PKA17, Fig. 1). This undoubtedly occurs because the continuous opacity beyond ~1.6 μm is much higher in the Sun than in a cool giant such as Arcturus, whose atmosphere is of low density. According to Figs. 8.3 and 8.5a,b of Gray (2005), the infrared continuum near 1.6 μm in both stars is formed at deep atmospheric levels because the H^- bound-free opacity, the major source of continuous opacity, has declined dramatically from its maximum at 8500 Å. Beyond 1.6 μm in a warm star like the Sun, but not in a cool giant like Arcturus, the H^- free-free opacity rises steadily through the optical and infrared. In the Sun, by 2.0 μm the total continuous opacity of the Sun again equals that at 5000 Å, i.e. at a depth where $\tau_{5000} = 1$, the benchmark depth for optical continuum formation. The H^- free-free opacity continues to rise continues at longer wavelengths, which drives solar line formation towards shallower, cooler levels.

In cool giants such as Arcturus, however, the low electron pressure greatly reduces the H^- free-free opacity, and lines continue to be formed at large depths. Greater depths have higher temperatures, which leads to stronger lines of highly-excited lines than expected for its effective temperature. This in turn suggests that highly-excited Fe I lines that are detectable in the solar spectrum should remain as strong in giants that are cooler and more luminous. This is indeed observed, as discussed in Section 9.

Molecular lines also have a significant presence in the infrared spectra of cool stars (e.g. Hinkle et al. 1995, Table 5). The line list adopted for molecular species is detailed in Section 5 of PKA17. These incorporate the gf-value corrections by band, rather than to individual lines. Disagreements between calculated and observed molecular-line strengths were modest, with the exception of CO lines.

Disagreements for infrared CO lines in the solar spectrum have been noted earlier, e.g. by Ayres & Testerman (1981) for the bands at 2200 and 4300 cm^{-1}. Both this work and Gray (2005) attributed the discrepancies to the enhanced formation of CO at low temperatures, coupled with the coexistence of hot and cold solar structures situated adjacent to one another at high atmospheric levels in the Sun. Indeed, images of the solar surface have long shown such structures as solar granulation (e.g. Title et al. 1989). Cheung et al. (2007) confirm that these are due to warm rising upflows, which in the Sun turn over at $\tau_{5000} = 0.3$ (a photospheric height 130 – 140 km above $\tau_{5000} = 1$), and, at the granulation boundaries, descend as cooler flows at higher speed to large depths. For Arcturus, the strengths of infrared CO lines, both at 4.7μm (e.g. Heasley et al. 1978; Wiedemann et al. 1994) and at 2.3μm (Ohnaka & Morales Marín 2018), also suggest one or more layers of cool gas at high atmospheric levels in inhomogeneous structures. Modeling these structures is beyond the scope of this investigation.

7. INFRARED SEARCH PROCEDURES

From Figure 1, it is evident that the unidentified Fe I jK lines are usually found in blends with other features. The gf-values of even very weak identified lines must be modified to assess the position and contribution of the identified feature to the blend. To do this across the entire span of the solar observations to the accuracy needed to match every known atomic transition is a daunting task. Furthermore, for CO it may be impossible to reach agreement using the 1D models adopted, due to the effect noted above of the spatial inhomogeneity of a convective atmosphere on CO line formation.

This extensive mismatch between calculated and observed spectra prevented the adoption of cross-correlation techniques to search for matched unidentified lines in this work. Cross-correlation techniques developed by Tonry & Davis (1979) have proven very effective in deriving radial velocities from spectral line shifts of individual spectra of stars in globular clusters (e.g. Peterson & Latham 1989; Peterson, Rees, & Cudworth 1995). Here, however, the persistent, systematic nature of the

mismatch has undesirable consequences. For example, each line whose strength is underestimated in the calculation generates a potential unidentified line to be matched. Masking individual lines from the cross-correlation is possible in principle, but infeasible with CO lines due to their high density and broad wavelength range (Hinkle et al. 1995, Table 5). Pending better modeling of the atomic and CO line strengths, the searches were conducted manually as before, following the earlier procedures.

Identifying jK levels is greatly simplified by the pattern of energies of levels within a particular jK group. Johansson et al. (1994) discussed this pattern as part of their determinations for levels of the s5g group of jK levels. Their Fig. 2 shows that the energies of s5g levels fall within five distinct bands of width 5 – 15 cm^{-1} separated by 100 – 400 cm^{-1}. The individual energies of the levels in each band occur in pairs whose angular momentum value J differs by 1. The mean energies of these pairs closely follow parabolas whose independent variable is constructed from j, K, and the angular momentum *l* of the orbiting electron. Armed with this prescription, they reproduced the line positions observed in laboratory spectra and in the ATMOS solar atlas to derive energies good to 0.01 cm^{-1} or better for 56 of the 58 levels present in the diagram. The two that escaped detection have the highest energies and the lowest J values. The scatter of the determined mean energies around each parabola is 0.02 cm^{-1}.

For this work we have exploited these relationships to determine energies for sixty unidentified levels in three jK configurations, those with core structure 4f, s5f, and s6f. Within each group of the same configuration, the total set of levels, known and unknown, was searched as a group. For the s6f group with no previous identifications, the first search was conducted for the energy of a level of high J in the lowest band. The spacing of two strong lines of this level with a modest difference in predicted wavenumbers was compared against observed spectra by finding two unidentified features with the identical spacing. Their mutual offset determined the shift of the predicted energy of that level to its actual energy, which was confirmed from its other detectable lines. This constrained the energies of each of the other levels of this band to typically ±4 cm^{-1}. Searches within such a narrow range proved successful after a minimum of trial and error. The search then proceeded to bands of successively higher energy, by again choosing a high-J level and initially assuming the same offset as that found for the band beneath. Once its own detectable lines accurately specified the offset of the targeted level, other levels in the band were again found within a narrow energy range.

Attention was also paid to the number of strong lines of a level for which no line was detected at a level five times weaker than the predicted line strength. Levels were accepted only if the number of line detections exceeded by two or more the number of such strong nondetections. For, in contrast to LS levels, the gf-values of jK levels are generally predicted quite accurately. They typically required an overall reduction of −0.3 or −0.4 dex, and the relative line gf values proved good to ±0.2 dex.

A new jK level energy was accepted if it fell within 1 cm^{-1} of the parabola of its band and led to three or more line matches. In some cases, gf-values of lines with wavelengths >6 μm, the limit of the spectral synthesis calculations, were high enough to suggest detectable lines in the ACE spectrum. Consequently, successful matches to the digital wavelengths of relatively isolated features in the ACE plot were accepted as well. As additional levels became established, the parabola was recalculated, and the conformity of the energies of less certain individual levels was re-examined.

Among the jK levels evaluated in the three 4f, s5f, and s6f groups were the 45 levels identified by N+94. Of the 45, only the seven levels listed in Table 1 failed to meet these criteria. Two were reconciled by a slight change in the energy, and one by adopting a significant energy change. Energies of the other four were dropped from the parabola fits and the quantum-mechanical calculations, as they gave rise to a large number of strong lines at positions where none was observed.

Both LS and jK searches lead to uncertainties of 0.01 – 0.02 cm^{-1} in the deduced energies, significantly larger than most laboratory measurements. This is due primarily to the lack of infrared lines in the LS levels, and to the blending of the jK lines in the stellar spectra. Compared to searches for LS levels, the jK searches are generally successful in shorter times, because the search for the energy of each jK level is limited to a much narrower range. Ambiguities do remain, however, especially when the width of a given band is narrow. Lines of similar energy and J overlap in wavelength and strength. The right energy may be assigned to the wrong level, and the resulting discrepancies may remain hidden due to low signal-to-noise, extreme line crowding, or telluric obliteration of critical wavelength regions.

8. RESULTS

Applying the above procedures to UV, optical, and infrared spectra has resulted in new identifications for a hundred Fe I levels. Table 2 presents the full label of each newly identified level, its conventional shortened from, the value of its angular momentum J, and its energy E in cm^{-1}. LS levels precede jK levels. Within each group, levels are listed in order of increasing J, then increasing E. For jK levels, the label gives the abbreviated base configuration of the core followed by its values of j and k, the latter in square brackets. Each of these values is indicated by an integer and a + sign, which stands for .5.

In all, one LS level of even parity and thirty-nine LS levels of odd parity, and sixty jK levels of odd parity, are newly identified. New identifications are thus presented for a total of one hundred levels.

An estimate of the number of detectable infrared lines these hundred levels may harbor can be derived following the gf-value correction approach of PKA17. Just as the gf-values of LS levels were corrected to the furnace temperature to account for the depletion of the population of the lower level of a transition as a function of its lower excitation energy E_{lo}, a similar corrected $\log S = \log gf - 0.877*E_{lo}$ can be invoked to account for the population at the solar photospheric temperature. Based on PKA17 and the new jK level detections, we count an infrared line as detectable if $\log S > -7.3$ for wavelengths from 1.12 to 2.26 μm, –7.5 over 2.26 – 5 μm, –7.0 over 5 – 8 μm, –6.5 over 8 – 11 μm, and –5.5 over 11 – 16 μm. Applying these criteria to the list presented here of newly-identified Fe I lines yields identifications for 143, 260, 201, 1, and 0 potentially detectable Fe I lines in each of these regions. This may be compared to the results of applying these criteria to the list of previously known Fe I lines, which results in 2606, 1968, 252, 64, and 8 known, potentially detectable Fe I lines in each of these regions. Among the previously known lines, jK levels accounted for 803, 508, 127, 1, and 1 lines. The jK level determinations are clearly very important in the 5 – 8 μm region, and have a significant presence over 2 – 5 μm as well.

9. STATUS AND POTENTIAL IMPACT OF Fe I LINE IDENTIFICATIONS

Table 3 presents a list of potentially detectable Fe I lines newly identified from the levels of Table 2, and their parameters and energy levels. It was generated by removing all lines with log gf < -6, and by removing lines with gf-values below progressively higher limits as a function of wavelength. The full table consists of nearly 40,000 Fe I lines from 157nm to 16 μm. It is an .mrt file associated with this paper online; its Readme file gives its format and the specific criteria for line removal. Table 3 in the printed version displays only the first twelve lines to illustrate its contents. The untrimmed lists of all lines at all wavelengths that originate from these levels, plus those of the revised levels in Table 1 and all other Fe I lines, are posted on the Kurucz website in subdirectory /atoms/2600. The file gf2600.lines incorporates all lines, including those involving levels with predicted energies whose wavelengths are highly uncertain (Sec. 2). The file gf2600.pos includes only lines that arise from two levels whose energies are both known, and whose wavelengths are thus suitable for high-resolution analysis.

Section 2 has outlined several areas of astrophysical research where the identification of numerous Fe I lines and levels can assist ongoing investigations. Here we describe the practical contributions of current and future identifications in two such areas: the modeling of UV fluxes and the reduction of systematic errors in the abundances of elements other than iron for warm stars of old stellar populations, and the determinations of abundances and abundance gradients for iron and the light elements from infrared spectra of cool, luminous giants.

Figure 1 of PK15 illustrates that before our identifications of Fe I levels began, spectral calculations seriously underestimated the spectral fluxes in the 2550 – 2700 Å region of all but the most metal-poor stars of solar temperature. As Peterson, Barbuy, and Spite (2020) demonstrated, this deficiency is directly attributable to unidentified Fe I lines arising from levels of high excitation. The current work on LS levels has helped to close the gap for warm metal-poor stars. However, the full benefit of such theoretical modeling is attained only when it reproduces the UV fluxes of the warm stars of solar metallicity. These are the stars that contribute the most UV flux in old solar-metallicity populations, which lack the hot blue horizontal branch stars of old, metal-poor populations. Their UV fluxes are thus sensitive to both metallicity and age: they are depressed as the iron content rises and absorbs more UV flux, but this also happens as old stellar systems age and the brightest warm stars become cool giants.

Modeling solar metallicity correctly in the UV is thus essential to derive age and metallicity determinations for old, quiescent galactic systems that are free from the long-standing ambiguity between age and metallicity (Worthey 1994). Some work has ventured towards incorporating the UV, but even the narrow-band Sloan *u* filter and its variants are centered near 350nm, where Fe I lines are outnumbered by lines of a variety of other species. Bringing UV modeling up to speed would take advantage of the specific sensitivity of the 2550 – 2700 Å region to the iron abundance, sharpening an essential tool for interpreting UV flux distributions observed at low resolution for many nearby galaxies. It could prove especially useful for disentangling age from metallicity and light-element enhancement in future JWST high-redshift targets, where the UV is shifted into the IR.

Because jK levels give rise to very few UV lines, further reducing the UV flux gap requires new LS identifications. Thanks to the improved constraints on the energies offered by the newly-identified LS and jK levels, and the inclusion of infrared spectra, such searches now appear feasible. This is true especially for levels with J=5 or higher, as the 2J+1 dependence of the statistical weight g (e.g. Eriksson & Lennerstad 2017) leads to higher gf-values and thus stronger lines. The Kurucz predicted calculations suggest that these should give rise to strong and isolated unidentified lines in the infrared.

Indeed, the current work has failed to identify a good many of the strongest unidentified infrared lines, notably those with wavelengths in the 1 – 2 μm range (e.g. Smith et al. 2021). The high-J states of Fe I occur in nf, ng, nh, and ni levels, which were not targeted in previous investigations because their predicted energies were frequently in error by 100 cm^{-1} or more. The new level identifications can now confine the search for additional high-J LS levels to a much narrower range. As an example, only one out of eighteen identified J=5 odd-parity levels with energies > 60000 cm^{-1} shows an offset > 100 cm^{-1}.

By focusing effort on jK lines, this work has contributed a significant number of Fe I identifications throughout the infrared (Sec. 8). Notably, it has nearly doubled the total number of Fe I lines identified in the 5 – 8 μm region. However, swarms of unidentified Fe I lines remain throughout the infrared. The 5f, s7f, and s7h jK groups of odd parity, and the 5g, s7g, and s7i jK groups of even parity, all have high-J levels whose bands overlap in energy with the jK energies identified here, and so can likely yield many more successful identifications.

Several areas of investigation would benefit. Improvements in the modeling of continuum placement and line blending in high-quality infrared spectra of stars like the Sun and red horizontal branch stars (e.g. Afşar et al. 2018, Fig. 3), would reduce systematic errors in abundance derivations of elements with few UV or optical lines. These include heavier elements past the iron peak represented primarily by UV lines (e.g. Peterson 2011; Roederer et al. 2016), and those whose infrared lines are weak but detectable (e.g. Cunha et al. 2017). Also included are lighter elements with sparse spectra such as fluorine (e.g. Jönsson et al. 2014; Pilachowski and Pace 2015; Abia et al. 2019) and phosphorus (e.g. Maas, Cescutti, & Pilachowski 2019). Heavy and light elements elucidate nucleosynthesis processes and environments at early epochs (Sneden et al. 2008), and the delayed contribution of evolved asymptotic giant-branch stars (Pilachowski & Pace 2015). Phosphorus is of special importance to astrobiology, as its relative abundance in a planetary host star influences prospects for life on its planet (Hinkel, Hartnett, & Young 2020).

Systematic errors in the infrared analysis of the iron abundance of cooler, stronger-lined red giants are also reduced by identifications of infrared Fe I lines. As discussed in Sec. 6.3, due to the reduction of the H^- free-free opacity in the low densities of giant atmospheres, highly-excited Fe I lines in infrared spectra of giants are expected to have the same or greater strength than do those in the solar spectrum. Consequently, the numbers in Sec. 8 of newly-detectable infrared lines in the Sun should also apply to spectra of cool but luminous giants. Observations confirm this: unidentified lines are widely present in infrared spectra of cool, luminous giants, even the coolest of these. Johansson et al. (1991) noted them in the spectrum of the cool K5 giant α Tau (Ridgway et al. 1984). Fig. 2 of García Pérez et al. (2015) reveals them as sharp peaks in the spectrum of the difference between the best spectral fit for a cool, solar-metallicity giant and its APOGEE spectrum. Fig. 3 of Ryde et al. (2016) shows 2 μm spectra for luminous red giants in the inner Galactic bulge, with many lines unmatched by spectral synthesis in the strongest-lined star.

The identification of the jK levels in Table 2, and additional groups of jK levels, should surely lead to more reliable infrared continuum placement in cool giants. Defining the infrared continuum is crucial where optical spectra are too faint to be obtained, such as in giants of the bulge, bar, and disk of the Milky Way (e.g. Ryde et al. 2016). This would provide more accurate abundances and abundance gradients of iron and the light-alpha elements, refining the understanding of the assembly and dissipation of these structures. Moreover, the improvement in estimates of reddening by Galactic dust (e.g. Schlafly et al. 2016) should assist interpretations of JWST bulge and distant infrared sources.

Acknowledgements. The solar NSO/Kitt Peak FTS data were produced by NSF/NOAO. We thank Frank Hill for assistance with obtaining them. We thank M. Afşar and C. Sneden for the spectrum of HD 95870 (HIP 54048). Support for Fe I identifications under program number HST-GO-15179 was provided to the authors through NASA grants from the Space Telescope Science Institute, which is operated by the association of Universities for Research in Astronomy (AURA), Inc. under NASA contract NAS 5-26555. Support for the infrared extension of Fe I identifications was provided by NASA grant 80NSSC19K0750. IRAF is distributed by the National Optical Astronomy Observatories, which are operated by the Association of Universities for Research in Astronomy, Inc., under cooperative agreement with the National Science Foundation.

FIGURE 1

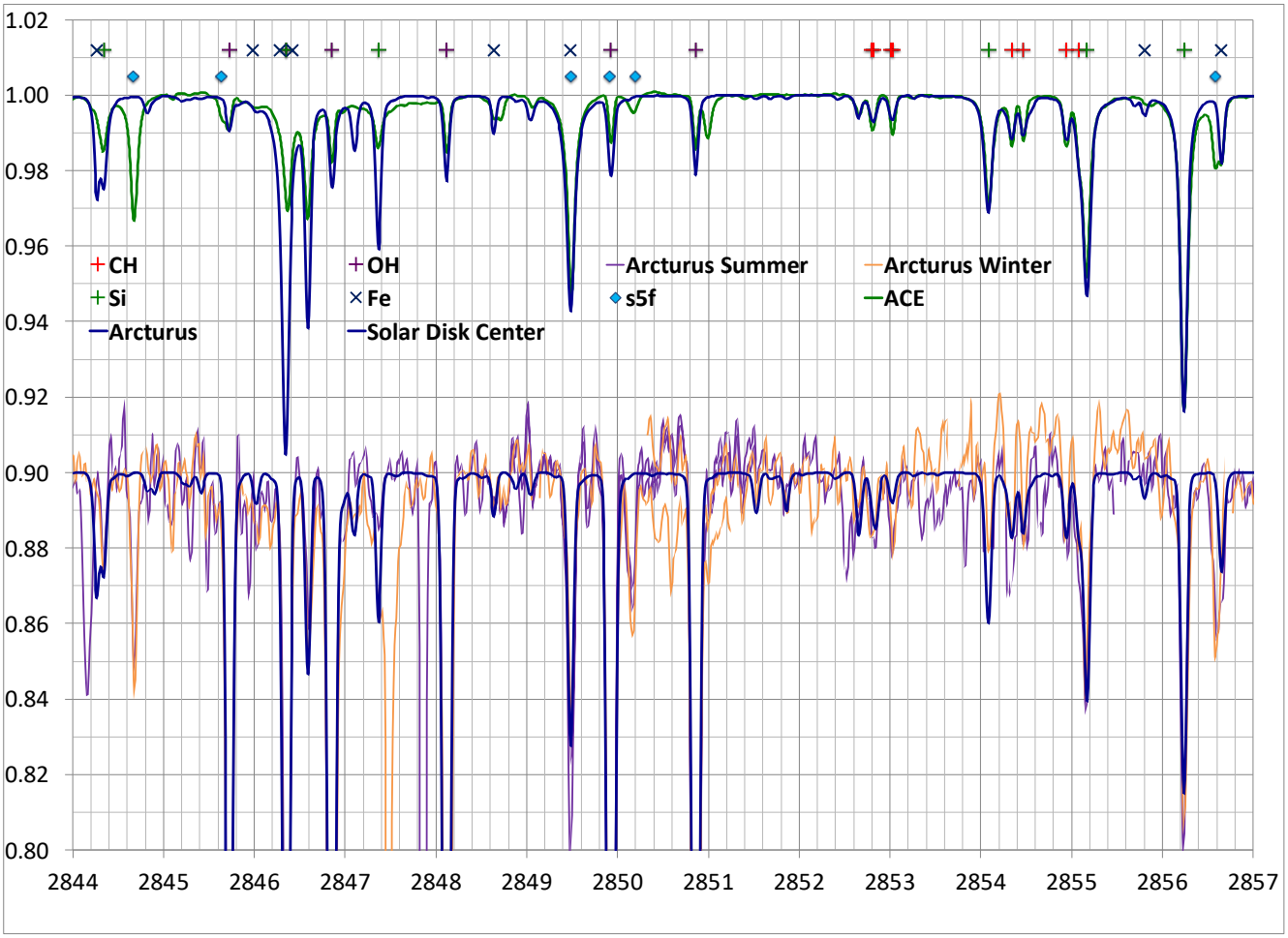

Figure 1. This figure compares observations versus calculations for the continuum-normalized intensity of the Sun and of the flux of Arcturus over 3.515 – 3.49μ. On the X-axis appears the wavenumber in cm^{-1}. On the Y-axis is the intensity scale for the solar spectrum; the Arcturus spectrum is offset vertically by –0.1 for clarity. The observed spectrum for the Sun is that of ACE (Hase et al. 2010; green line). For Arcturus are shown both the Winter (orange line) and Summer (purple line) spectra of Hinkle et al. (1995). Superimposed as solid blue lines are spectral synthesis calculations (Sec. 6.2) for the center of the solar disk and the integrated flux of Arcturus. The positions of selected lines of molecular and neutral atomic species are indicated by × for Fe I and by color-coded + signs for the other species indicated. The diamonds beneath them highlight Fe I lines that arise from s5f jK levels. The s5f line at 2849.5 cm^{-1} was previously identified by Nave et al. (1994). The remaining five s5f lines, which fall above observed features that are unmatched except for line blends, are new identifications.

REFERENCES

Abia, C., Cristallo, S., Cunha, K., de Laverny, P, & Smith, V.V. 2019, A&A, 625, 40

Abrams, M.C., Goldman, A., Gunson, M.R., Rinsland, C.P., & Zander, R. 1996, Appl. Opt., 35, 2747.

Afşar, M., Sneden, C., Wood, M.P., Lawler, J.E., et al. 2018, ApJ, 865, 44

Ayres, T.R., & Testerman, L. 1981, ApJ, 245, 1124

Barbuy, B., Chiappini, C., & Gerhard, O. 2018, ARA&A, 56, 223

Brown, C.M., Ginter, M.L., Johansson, S., & Tilford, S.G. 1988, JOSA B, 5, 2125 (B+88)

Castelli, F., & Kurucz, R.L. 2003, IAU Symp. No 210, "Modeling of Stellar Atmospheres", eds. N. Piskunov et al., CD-ROM poster A20; also astro-ph 0405087; ODFNEW models are at http://Kurucz.harvard.edu/grids/ and http://wwwuser.oat.ts.astro.it/castelli/grids.html

Castelli, F., & Kurucz, R.L. 2010, A&A, 520, 57

Cheung, M.C.M., Schüssler, M., & Moreno-Insertis, F. 2007, A&A, 461, 1163

Cowan, R.D. 1981, *The Theory of Atomic Structure and Spectra*, Los Alamos Series in Basic and Applied Sciences, Berkeley, University of California Press

Cunha, K., Smith, V.V., Hasselquist, S., Souto, D., et al. 2017, ApJ, 844, 145

Eriksson, M., & Lennerstad, H. 2017, JPhCS, 869, 012010

Farmer, C.B., & Norton, R.H. 1989, "A high resolution atlas of the Infrared spectrum of the sun and the earth atmosphere from space. vol. I. The Sun", NASA Reference Publication 1224, Washington DC: National Aeronautics and Space Administration.

García Pérez, A.E., Allende Prieto, C., Holtzman, J.A., Shetrone, M., et al. 2015, AJ, 151, 144

Gray, D.F. 2005, *The observation and analysis of stellar photospheres*, 3rd edition, Cambridge University Press.

Hase, Frank, Wallace, F., McLeod, S.D., Harrison, J.J., & Bernath, P.F. (2010), JQSRT, 111, 521

Heasley, J. N., Ridgway, S. T., Carbon, D.F., Milkey, R.W., & Hall, D.N.B. 1978, ApJ, 219, 970

Hinkel, N.R., Hartnett, H.E., & Young, P.A. 2020, ApJL, 900, 38

Hinkle, K., Wallace, L., & Livingston, W. 1995, "Infrared Atlas of the Arcturus Spectrum 0.9 – 5.3μm" (ASP: San Francisco)

Hinkle, K., Wallace, L., Valenti, J., & Harmer, D. 2000, "Visible and Near Infrared Atlas of the Arcturus Spectrum 3727 – 9300Å" (ASP: San Francisco)

Johansson, S., Nave, G., Geller, M., Sauval, A.G., et al. 1994, ApJ, 429, 419

Johansson, S., Nave, G., Learner, R.C.M., & Thorne, A.P. 1991, in *The Infrared Spectral Region of Stars*, ed. C. Jaschek & Y. Andrillat (Cambridge: Cambridge Univ. Press), 189

Jönsson, H., Ryde, N, Harper, G.M., Cunha, K., et al. 2014, A&A, 564, A122

Käufli, H.-U., Ballester, P., Biereichel, P., et al. 2004, Proc. SPIE, 5492, 1218

Kurucz, R.L. 1993, CD-ROM 18, SYNTHE Spectrum Synthesis Programs and Line Data (Cambridge: Smithsonian Astrophys. Obs.); at http://Kurucz.harvard.edu/

Kurucz, R.L. 2011, Can. J. Phys., 80, 417

Kurucz, R.L. 2017, Can. J. Phys., 85, 825

Kurucz, R.L. 2018, ASPC, 515, 47

Maas, Z.G., Cescutti, G., & Pilachowski, C.A. 2019, AJ, 158, 219

Maiolino, R., Haehnelt, M., Murphy, M.T., et al. 2013, arXiv:1310.3163

Majewski, S.R., Schiavon, R.P, Frinchaboy, P.M., et al. 2017, AJ, 154, 94

Matteucci, F. 2021, A&ARv, 29, 5

Moore, C.E., Minnaert, M.G.J., & Houtgast, J. 1966, *The Solar Spectrum 2935 Å to 8770 Å*, NBS Monograph No. 61

Nave, G., & Johansson, S. 1993a, A&A, 274, 961

Nave, G., & Johansson, S. 1993b, A&AS, 102, 269

Nave, G., Johansson, S., Learner, R.C.M., Thorne, A.P, & Brault, J.W. 1994, ApJS, 94, 221 (N+94)

Ohnaka, K., & Morales Marín, C.A.L. 2018, A&A, 620, A23
Peterson, R.C. 2011, ApJ, 742, 21
Peterson, R.C. 2021, ApJL, 914, 22
Peterson, R.C., Barbuy, B., & Spite, M. 2020, A&A, 638, A64
Peterson, R.C., Dalle Ore, C.M., & Kurucz, R.L. 1993, ApJ, 404 333
Peterson, R.C., & Kurucz, R.L. 2015, ApJS, 216, 1 (PK15)
Peterson, R.C., Kurucz, R.L., & Ayres, T.R. 2017, ApJS, 229, 23 (PKA17)
Peterson, R.C., & Latham, D.W. 1989, ApJ, 336, 178
Peterson, R.C., Rees, R.F., & Cudworth, K.M. 1995, ApJ, 443, 124
Pilachowski, C.A., & Pace, C. 2015, AJ, 150, 66
Ridgway, S.T., Carbon, D.F., Hall, D.N.W., & Jewell, J. 1984, ApJS, 54, 177
Roederer, I.U., Karakas, A.I., Pignatari, M., & Herwig, F. 2016, ApJ, 821, 37
Ryde, N., Schultheis, M., Grieco, V., Matteucci, F., Rich, R.M., & Uttenhaler, S. 2016, AJ, 151, 1
Schlafly, E.F., Meisner, A.M., Stutz, A.M., Kainulainen, J., et al. 2016, ApJ, 821, 78
Schoenfeld, W.G., Chang, E.S., Geller, M., Johansson, S., et al. 1995, A&A, 301, 583
Smith, V.V., Bizyaev, D., Cunha, K., Shetrone, M.D., et al. 2021, AJ, 161, 254
Sneden, C., Cowan, J.J., & Gallino, R. 2008, ARA&A, 46, 241
Title, A.M., Tarbell, T.D., Topka, K.P., et al. 1989, ApJ, 336, 475
Tonry, J., & Davis, M. 1979, AJ, 84, 1511
Tousey, R. 1988, JOSA B, 5, 2230
Vogt, S.S., Allen, A.L., Bigelow, B.C., et al. 1994, SPIE, 2198, 362
Wallace, L., Hinkle, K., & Livingston, W. 1993, "An Atlas of the Photospheric Spectrum from 8900 to 13600 cm^{-1} (7350 to 11230 Å)", N.S.O. Technical Report #93-001, April 1993
Wallace, L., Hinkle, K. H., Livingston, W. C., & Davis, S. P. 2011, ApJS, 195, 6
Wallace, L., & Livingston, W. 2003, "An Atlas of the Solar Spectrum in the Infrared from 1850 to 9000 cm^{-1} (1.1 to 5.4 μm)", Tucson: National Solar Observatory, National Optical Astronomy Observatory, NSO Technical Report 03-001
Wiedemann, G., Ayres, T.R., Jennings, D.E., & Saar, S.H. 1994, ApJ, 423, 806
Worthey, G. 1994, ApJS, 95, 107

TABLE 1

Revised Fe I Levels and Energies

Expanded Label	Label	J	E (cm^{-1})	Former E (cm^{-1})	Reference
LS Levels:					
Three Even Levels:					
3d6 4s(6D)8s 5D	4s6D8s 5D	3	Drop	60078.83	PKA17
3d7(2G)4d 3I	(2G)4d 3I	6	67185.97	67245.33	PKA17
3d7(2G)4d 3I	(2G)4d 3I	7	67167.93	67167.95	PKA17
jK Levels:					
Seven Odd Levels:					
d7(4D)4f 2+[2+]	4f 2+[2+]	2	Drop	59680.306	N+94
d7(4D)4f 4+[3+]	4f 4+[3+]	3	Drop	58714.648	N+94
d7(4D)4f 1+[4+]	4f 1+[4+]	4	Drop	59960.956	N+94
d7(4D)4f 4+[5+]	4f 4+[5+]	5	58700.81	58700.834	N+94
d7(4D)s5f 3+[5+]	s5f 3+[5+]	5	Drop	59663.964	N+94
d7(4D)s5f 4+[6+]	s5f 4+[6+]	6	59280.56	59275.884	N+94
d7(4D)s5f 3+[6+]	s5f 3+[6+]	6	59670.06	59670.084	N+94

TABLE 2

New Fe I Levels and Energies

Expanded Label	Label	J	E (cm^{-1})
LS Levels:			
One Even Level:			
3d7(4F)5d 5H	(4F)5d 5H	5	59687.88
39 Odd Levels:			
d6(5D)4s(6D)5p 5D	4s6D5p 5D	0	58556.38
d7(4F)6p 5F	(4F)6p 5F	1	59761.68
d6(5D)4s(6D)7p 5P	4s6D7p 5P	1	60253.31
d6(5D)4s(6D)8p 7D	4s6D8p 7D	1	61266.98
d6(5D)4s(6D)8p 5P	4s6D8p 5P	1	61621.21
d6(5D)4s(6D)9p 5D	4s6D9p 5D	1	62103.84
d7(4F)7p 5F	(4F)7p 5F	1	62417.13

d7(4F)7p 3D	(4F)7p 3D	1	62666.97
d6(5D)4s(4D)5p 3F	4s4D5p 3F	2	58483.58
d6(5D)4s(6D)7p 7D	4s6D7p 7D	2	59632.62
d6(5D)4s(6D)7p 5F	4s6D7p 5F	2	60099.96
d6(5D)4s(6D)8p 7D	4s6D8p 7D	2	60999.34
61023o	61023o	2	61023.23
d6(5D)4s(6D)8p 5D	4s6D8p 5D	2	61208.17
d6(5D)4s(6D)8p 7F	4s6D8p 7F	2	61285.50
d6(5D)4s(6D)8p 5P	4s6D8p 5P	2	61432.02
d6(1D)4s4p(3P) 3P	1Dsp3P 3P	2	61826.24
d6(5D)4s(6D)9p 5P	4s6D9p 5P	2	62201.85
d7(4F)7p 5F	(4F)7p 5F	2	62273.34
d6(5D)4s(6D)9p 7P	4s6D9p 7P	2	62326.92
d7(4F)7p 3D	(4F)7p 3D	2	62331.33
d6(5D)4s(6D)10p 7D	4s6D10p 7D	2	62386.97
d6(5D)4s(6D)7p 7D	4s6D7p 7D	3	59339.26
d6(5D)4s(6D)7p 7F	4s6D7p 7F	3	59503.40
d6(5D)4s(6D)8p 5D	4s6D8p 5D	3	61012.24
d6(5D)4s(6D)9p 5P	4s6D9p 5P	3	61476.76
d6(5D)4s(6D)9p 7P	4s6D9p 7P	3	62087.91
d6(5D)4s(6D)9p 7F	4s6D9p 7F	3	62268.60
d7(4F)6p 5F	(4F)6p 5F	4	59117.74
d6(5D)4s(6D)8p 5D	4s6D8p 5D	4	60628.77
d6(5D)4s(6D)8p 7F	4s6D8p 7F	4	61173.80
d7(4F)7p 5D	(4F)7p 5D	4	61232.91
d6(5D)4s(6D)10p 5F	4s6D10p 5F	4	62537.38
d7(3G)4s4p(3P) 3H1	3Gsp1P 3H1	4	63501.17
d6(3G)4s4p(1P) 3H2	3Gsp1P 3H2	4	63571.96
d7(4F)7p 5G	(4F)7p 5G	6	61173.01
d6(3H)4s4p(3P) 5I	3Hsp3P 5I	7	42880.56
d6(3H)4s4p(3P) 5H	3Hsp3P 5H	7	43348.46
d6(3H)4s4p(3P) 5I	3Hsp3P 5I	8	43099.26

jK Levels:

60 Odd Levels:

d6(5D)4s(6D)4f 2+[0+]	s4f 2+[0+]	0	57420.84
d7(4F)4f 3+[1+]	4f 3+[1+]	1	59270.59
d6(5D)4s(6D)5f 4+[1+]	s5f 4+[1+]	1	59297.42
d6(5D)4s(6D)6f 4+[1+]	s6f 4+[1+]	1	60658.52
d6(5D)4s(6D)6f 3+[0+]	s6f 3+[0+]	1	61037.83
d6(5D)4s(6D)6f 2+[1+]	s6f 2+[1+]	1	61316.46
d6(5D)4s(6D)5f 4+[1+]	s5f 4+[1+]	2	59297.38
d6(5D)4s(6D)5f 3+[2+]	s5f 3+[2+]	2	59668.53
d6(5D)4s(6D)5f 2+[2+]	s5f 2+[2+]	2	59955.05

d6(5D)4s(6D)5f 1+[1+]	s5f 1+[1+]	2	60141.46
d6(5D)4s(6D)5f 1+[2+]	s5f 1+[2+]	2	60150.82
d6(5D)4s(6D)6f 4+[2+]	s6f 4+[2+]	2	60654.52
d6(5D)4s(6D)6f 4+[1+]	s6f 4+[1+]	2	60657.10
d6(5D)4s(6D)6f 3+[2+]	s6f 3+[2+]	2	61036.11
d6(5D)4s(6D)6f 3+[1+]	s6f 3+[1+]	2	61037.02
d6(5D)4s(6D)6f 2+[2+]	s6f 2+[2+]	2	61319.92
d6(5D)4s(6D)6f 0+[2+]	s6f 0+[2+]	2	61626.82
d6(5D)4s(6D)5f 2+[3+]	s5f 2+[3+]	3	59954.48
d6(5D)4s(6D)5f 2+[2+]	s5f 2+[2+]	3	59956.10
d6(5D)4s(6D)5f 1+[2+]	s5f 1+[2+]	3	60147.82
d6(5D)4s(6D)5f 1+[3+]	s5f 1+[3+]	3	60153.56
d6(5D)4s(6D)5f 0+[2+]	s5f 0+[2+]	3	60260.28
d6(5D)4s(6D)5f 0+[3+]	s5f 0+[3+]	3	60262.24
d6(5D)4s(6D)6f 4+[3+]	s6f 4+[3+]	3	60650.19
d6(5D)4s(6D)6f 4+[2+]	s6f 4+[2+]	3	60653.66
d6(5D)4s(6D)6f 1+[3+]	s6f 1+[3+]	3	61523.65
d6(5D)4s(6D)6f 0+[3+]	s6f 0+[3+]	3	61627.26
d6(5D)4s(6D)5f 4+[3+]	s5f 4+[3+]	4	59283.87
d6(5D)4s(6D)5f 3+[3+]	s5f 3+[3+]	4	59667.29
d6(5D)4s(6D)5f 2+[3+]	s5f 2+[3+]	4	59953.89
d6(5D)4s(6D)5f 1+[4+]	s5f 1+[4+]	4	60143.31
d6(5D)4s(6D)5f 1+[3+]	s5f 1+[3+]	4	60152.95
d6(5D)4s(6D)5f 0+[3+]	s5f 0+[3+]	4	60260.45
d6(5D)4s(6D)6f 4+[4+]	s6f 4+[4+]	4	60646.88
d6(5D)4s(6D)6f 4+[3+]	s6f 4+[3+]	4	60648.91
d6(5D)4s(6D)6f 3+[3+]	s6f 3+[3+]	4	61034.35
d6(5D)4s(6D)6f 2+[4+]	s6f 2+[4+]	4	61319.16
d6(5D)4s(6D)6f 0+[3+]	s6f 0+[3+]	4	61626.10
d6(5D)4s(6D)5f 4+[5+]	s5f 4+[5+]	5	59276.69
d6(5D)4s(6D)5f 4+[4+]	s5f 4+[4+]	5	59280.61
d6(5D)4s(6D)5f 3+[4+]	s5f 3+[4+]	5	59666.81
d6(5D)4s(6D)5f 2+[5+]	s5f 2+[5+]	5	59949.47
d6(5D)4s(6D)5f 1+[4+]	s5f 1+[4+]	5	60142.00
d6(5D)4s(6D)6f 4+[5+]	s6f 4+[5+]	5	60645.39
d6(5D)4s(6D)6f 4+[4+]	s6f 4+[4+]	5	60646.34
d6(5D)4s(6D)6f 3+[4+]	s6f 3+[4+]	5	61033.58
d6(5D)4s(6D)6f 3+[5+]	s6f 3+[5+]	5	61033.70
d6(5D)4s(6D)6f 2+[5+]	s6f 2+[5+]	5	61316.16
d6(5D)4s(6D)6f 2+[4+]	s6f 2+[4+]	5	61317.97
d6(5D)4s(6D)5f 3+[5+]	s5f 3+[5+]	6	59666.41
d6(5D)4s(6D)5f 2+[5+]	s5f 2+[5+]	6	59948.11
d6(5D)4s(6D)6f 4+[5+]	s6f 4+[5+]	6	60644.57
d6(5D)4s(6D)6f 4+[6+]	s6f 4+[6+]	6	60647.32
d6(5D)4s(6D)6f 3+[5+]	s6f 3+[5+]	6	61033.59

d6(5D)4s(6D)6f 3+[6+]	s6f 3+[6+]	6	61034.68
d6(5D)4s(6D)6f 2+[5+]	s6f 2+[5+]	6	61315.77
d6(5D)4s(6D)6f 4+[6+]	s6f 4+[6+]	7	60646.33
d6(5D)4s(6D)6f 4+[7+]	s6f 4+[7+]	7	60653.92
d6(5D)4s(6D)6f 3+[6+]	s6f 3+[6+]	7	61035.01
d6(5D)4s(6D)6f 4+[7+]	s6f 4+[7+]	8	60653.96

Note. The Kurucz website in the subdirectory /atoms/2600 contains the log files from the least squares fits, b2600e.log and b2600o.log, which list the three largest eigenvector components for each level.

TABLE 3

Newly Classified Lines of Fe I

Wavelength (nm)	log gf	dgf	E_even (cm^{-1})	J_e	Label_e	E_odd (cm^{-1})	J_o	Label_o	Γ_R	Γ_S	Γ_W
158.2708	-4.934	...	0	4	4s2 a5D	63182.86	4	(4F)8p 3G	7.99	-3.41	-6.94
159.3696	-4.303	...	0	4	4s2 a5D	62747.24	4	4s6D10p 7F	7.41	-3.05	-6.79
159.5309	-5.035	...	0	4	4s2 a5D	62683.77	4	8p 3G5G5F	8.20	-3.21	-7.01
159.5522	-4.783	...	0	4	4s2 a5D	62675.42	5	(4F)8p 5G	7.75	-2.65	-6.96
159.5946	-2.934	...	0	4	4s2 a5D	62658.78	3	4s6D10p 5D	7.99	-3.33	-6.82
159.6551	-3.559	...	0	4	4s2 a5D	62635.02	3	4s6D10p 7F	7.52	-2.63	-6.79
159.9750	-4.916	...	0	4	4s2 a5D	62509.75	3	(4F)8p 3F	8.17	-3.89	-7.02
160.0798	-4.747	...	415.933	3	4s2 a5D	62884.79	3	(4F)8p 3F	8.25	-3.06	-7.02
160.1728	-4.224	...	415.933	3	4s2 a5D	62848.51	2	(4F)8p 3D	7.98	-3.44	-6.91
160.1907	-5.090	...	415.933	3	4s2 a5D	62841.54	2	(4F)8p 3F	8.01	-3.26	-6.97
160.3156	-3.234	...	0	4	4s2 a5D	62376.97	4	(4F)8p 5D	7.03	-3.39	-6.92
160.4330	-1.414	...	415.933	3	4s2 a5D	62747.24	4	4s6D10p 7F	7.41	-3.05	-6.79

Note. Table 3 is published in its entirety in the electronic edition of The Astrophysical Journal Supplement Series. A portion is shown here for guidance regarding its form and content.